Journal of Crystal Growth 325 (2011) 93–95

Contents lists available at ScienceDirect

Journal of Crystal Growth

journal homepage: www.elsevier.com/locate/jcrysgro

Realization of non-polar ZnO (1 1 $\bar{2}$ 0) homoepitaxial films with atomically smooth surface by molecular beam epitaxy

T.C. Zhang [a,b], Z.X. Mei [a,*], A.Yu. Kuznetsov [b], X.L. Du [a,*]

[a] Beijing National Laboratory for Condensed Matter Physics, Institute of Physics, Chinese Academy of Sciences, Beijing 100190, China
[b] Department of Physics, University of Oslo, P.O. Box 1048 Blindern, NO-0316 Oslo, Norway

ARTICLE INFO

Article history:
Received 14 January 2011
Received in revised form
21 April 2011
Accepted 22 April 2011
Communicated by E. Calleja
Available online 10 May 2011

Keywords:
A1. Atomic force microscopy
A1. Non-polar ZnO
A1. Reflection high-energy electron diffraction
A3. Molecular beam epitaxy

ABSTRACT

A route for realizing non-polar ZnO (1 1 $\bar{2}$ 0) films with atomically smooth surface is demonstrated by employing rf-plasma assisted molecular beam epitaxy on ZnO bulk substrates. It is found that high growth temperature plays an important role in suppressing the typical striped structure along ZnO [0 0 0 1] direction on non-polar planes. An atomically smooth surface with a root mean square roughness of 0.51 nm that is suitable for fabrication of quantum wells is achieved after solving the growth anisotropy problem, as confirmed by the combined studies of reflection high-energy electron diffraction and atomic force microscopy.

1. Introduction

As an important II–VI semiconductor, ZnO has attracted much interest for its potential applications in wide range of fields such as gas sensors [1], catalysts [2] and acoustic devices [3]. Owing to its wide band gap (3.37 eV at room temperature) and large exciton bonding energy (60 meV), ZnO is considered as an excellent candidate for short wavelength optoelectronic devices and light-emitting diodes (LEDs) for example. With wurtzite crystal structure, ZnO films have been usually grown with (0 0 0 1) orientation in the growth direction [4–8]. In this case the presence of a built-in electrostatic field along this orientation, generated by spontaneous and piezoelectric polarizations, will result in the quantum confined Stark effect and poor electron–hole overlap in a quantum well structure, and give rise to a decrease of the luminous efficiency [9–11]. Therefore growth of non-polar ZnO, *A*-plane mostly, has been drawing an increasing attention in order to eliminate the influence of the internal electrostatic field on internal quantum efficiency of the LED devices. Significant efforts have been devoted to both heteroepitaxy [12] and homoepitaxy [13,14] of non-polar ZnO on different substrates recently, most of the films exhibit rough surfaces with typical striped structures and it is impossible to apply them to quantum well structures. For these applications, it is essential to improve the surface morphology and make it meet device requirements.

In this study, we mainly focus on the synthesis of non-polar ZnO films with atomically smooth surface grown on ZnO (1 1 $\bar{2}$ 0) substrates by rf-plasma assisted molecular beam epitaxy (rf-MBE). The influence of growth temperature has been explored and the growth anisotropy has been greatly depressed, as confirmed by reflection high-energy electron diffraction (RHEED) observations and atomic force microscopy (AFM) characterization.

2. Experiment

Homoepitaxial ZnO films were grown on non-polar (1 1 $\bar{2}$ 0) plane of commercial bulk ZnO single crystals by the rf-MBE method. Elemental Zn (7N) evaporated from a commercial Knudsen cell and active oxygen radicals produced by a rf-plasma system were supplied as sources. After degreasing in acetone and ethanol the substrates were thermally cleaned at 700 °C for 20 min, followed by exposure to active oxygen radicals at 600 °C for 20 min with a rf power of 320 W and an oxygen flux of 2.0 sccm. Then, a regular two-step growth process was performed with a low temperature buffer layer grown at 500 °C and a high temperature epilayer at 600–720 °C. Four samples were chosen for comparison (labeled as A, B, C and D), which were grown at 600, 600, 690 and 720 °C for 60, 120, 180 and 180 min,

* Corresponding authors. Tel.: +86 10 82648062; fax: +86 10 82649542.
E-mail addresses: zxmei@aphy.iphy.ac.cn (Z.X. Mei), xldu@aphy.iphy.ac.cn (X.L. Du).

0022-0248/$ - see front matter © 2011 Elsevier B.V. All rights reserved.
doi:10.1016/j.jcrysgro.2011.04.037

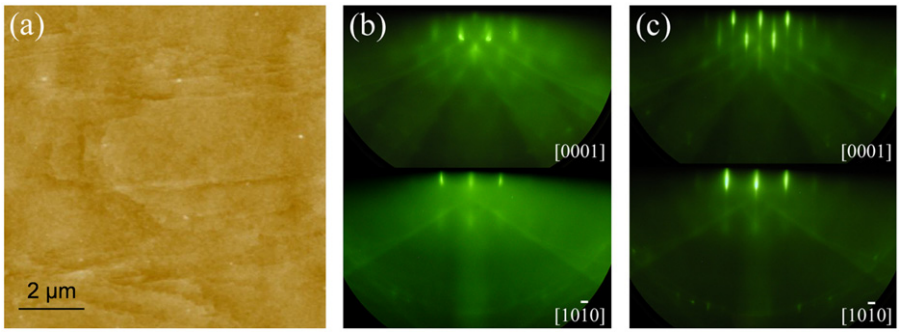

Fig. 1. AFM images of (a) ZnO (1 1 $\bar{2}$ 0) substrate and (b) and (c) are the RHEED patterns of the substrate before and after pretreatments, respectively.

respectively. The whole processes were monitored in situ by RHEED, and the surface morphologies were characterized by AFM.

3. Results and discussion

High-temperature thermal cleaning combined with exposure to oxygen plasma was chosen as pretreatment to improve the surface crystallinity of commercial ZnO bulk substrates before homoepitaxy. Fig. 1(a) shows the AFM image of the ZnO (1 1 $\bar{2}$ 0) substrate. The surface looks very smooth, which can be confirmed from the small root mean square (RMS) value in a $10 \times 10\ \mu m^2$ area (0.16 nm). A uniform surface morphology created by mechanical polish can be found without any indication of striped features. However, existence of some scratches caused by the polishing process can be clearly observed. The atoms in these damaged layers are distorted, and even missing from their regular positions. Fig. 1(b) and (c) exhibits RHEED patterns of the substrate before and after pretreatment, respectively. The diffuse spots with a low contrast against the background indicate the deviation of the surface atoms from the lattice points as mentioned above. Impurities adsorbed on the surface can be considered as another reason for this [Fig. 1(b)]. To remove the damaged layers and impurities, thermal cleaning of the surface at high temperature followed by oxygen plasma pretreatment is adopted before the homoepitaxial growth. The improved brightness and contrast of the elongated spots demonstrate the obvious preconditioning effects as seen in Fig. 1(c).

Stripes along *c*-axis are observed on both surfaces of samples A and B grown at 600 °C, which have been reported as a typical pattern on *A*-plane (1 1 $\bar{2}$ 0) ZnO [12–15]. Fig. 2(a) and (b) displays the top views of their AFM images in a $2 \times 2\ \mu m^2$ area. The roughness in a $10 \times 10\ \mu m^2$ area is 2.2 and 1.6 nm for A and B, respectively. Such an anisotropic morphology is caused by the difference of growth rates along different directions. It is well known that the asymmetry along *c*-axis in wurtzite structure results in polarization with an internal electrostatic field, which makes *c*-direction special. The growth velocity along [0 0 0 1] direction is supposed to be the largest owing to the highest surface energy in polar (0 0 0 1) plane [16–18]. Therefore the nucleus that originally formed on the surface exhibits a tendency to grow parallel to *c*-axis, and finally forms short rods laid on the surface, as shown in Fig. 2(a) and (b). Surface plots of sample A and B corresponding to (a) and (b) are shown in Fig. 2(c) and (d), respectively. The coalescence of these rods can be observed clearly. With increasing growth time, both the length and width of the rods increase and the numeral density decreases. Most of the rods laid on the surface connect to each other longitudinally and laterally, making them longer and broader, and finally show a stripe-like structure. The insets in Fig. 2(a) and (b) give the cross section profiles along the cutting lines of sample A and B,

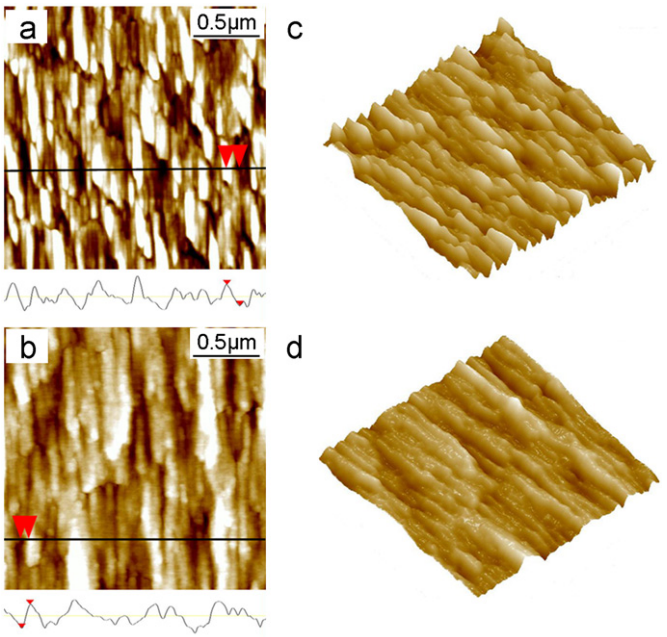

Fig. 2. AFM images in a $2 \times 2\ \mu m^2$ area of (a), (b) top views and (c), (d) surface plots of samples A and B grown at 600 °C for 60 and 120 min, respectively. The insets in (a) and (b) show the cross section profiles along the cutting lines of samples A and B, respectively.

respectively. The vertical distance between the two triangular marks is 7.9 and 4.5 nm for A and B, respectively, indicating a typical height of the peaks. It is found that further growth reduces the fluctuation of the surface, resulting in a smoother morphology to some extent. However the growth anisotropy along *c*-axis still occurs at the same growth temperature, which implies the necessity of a higher growth temperature.

AFM images in 10×10 and $2 \times 2\ \mu m^2$ areas of sample C grown at 690 °C are shown in Fig. 3(a) and (b), respectively. As presented in Fig. 3(a) a step-like structure forms, and the roughness is reduced to 1.0 nm. More details can be found in Fig. 3(b), in which the inset gives the cross section profile along the cutting line. The vertical distance between the two triangular marks is 2.2 nm, which is much lower than that of samples A and B. Growth along *c*-direction is not dominant due to the higher growth temperature. The migration length of the arriving Zn atoms is greatly enlarged at this temperature, which enables them to extensively bond with oxygen atoms at more energetically favorable sites. As a result the tendency to grow along [0 0 0 1] is depressed and the roughness is reduced, though growth anisotropy still occurs for these steps. The totally different structure with a relatively flat surface demonstrates a change of the growth behavior at higher temperature.

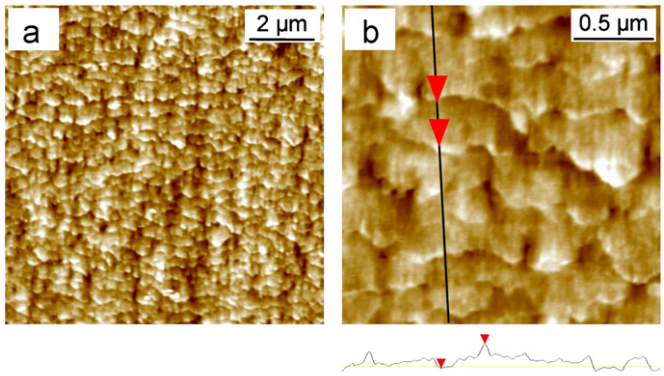

Fig. 3. AFM images in (a) $10 \times 10\ \mu m^2$ and (b) $2 \times 2\ \mu m^2$ area of sample C grown at 690 °C for 180 min. The inset in (b) shows the cross section profile along the cutting line.

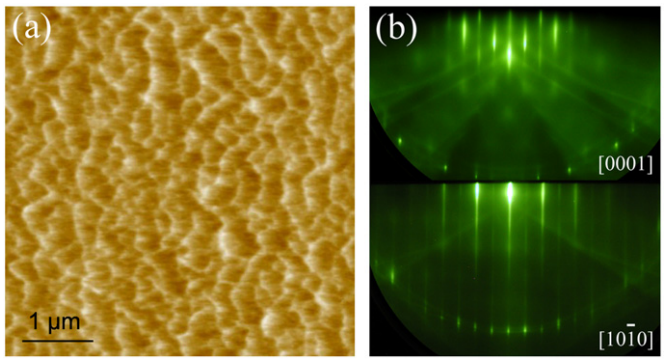

Fig. 4. AFM images in a $5 \times 5\ \mu m^2$ area of (a) top view and (b) RHEED patterns of sample D grown at 720 °C for 180 min.

To further explore the temperature-dependent evolution of surface morphology, the growth temperature was increased much higher. Fig. 4(a) shows AFM images of sample D grown at 720 °C for 180 min in a $5 \times 5\ \mu m^2$ area. As is shown in the figure, a uniform wave-like feature with almost no anisotropy is observed instead of the oriented steps. The fluctuation of the surface is reduced further, which leads to a RMS roughness of 0.51 nm in a $10 \times 10\ \mu m^2$ area.

Fig. 4(b) exhibits the RHEED patterns of sample D with incident electron beams along [0 0 0 1] and [1 0 $\bar{1}$ 0]. Compared with Fig. 1(c) the spots turn to sharp bright stripes with a high contrast to the background, and a 1×2 surface reconstruction appears, both of which indicate the achievement of a clean and smooth surface. Combined with the AFM images, the results present that the typical striped pattern on ZnO (1 1 $\bar{2}$ 0) plane is greatly depressed and a uniform atomically smooth surface can be realized at high growth temperature.

4. Conclusion

Non-polar ZnO (1 1 $\bar{2}$ 0) films were achieved homoepitaxially on ZnO (1 1 $\bar{2}$ 0) substrates by rf-MBE. The influence of growth temperature on the surface morphologies was investigated. A typical stripe-like structure along [0 0 0 1] direction was observed at low temperature, resulting in a rough surface. The surface morphology can be changed and the anisotropy can be depressed by adopting high growth temperature. An atomically smooth ZnO surface with a RMS roughness of 0.51 nm is realized, which makes it possible to fabricate quantum well structures based on non-polar ZnO materials.

References

[1] Travis Anderson, Fan Ren, Stephen Pearton, Byoung Sam Kang, Hung-Ta Wang, Chih-Yang Chang, Jenshan Lin, Sensors 9 (2009) 4669.
[2] A. Nageswara Rao, B. Sivasankar, V. Sadasivam, J. Hazard. Mater. 166 (2009) 1357.
[3] Linh Mai, Van-Su Pham, Giwan Yoon, Appl. Phys. A 95 (2009) 667.
[4] D.M. Bagnall, Y.F. Chen, Z. Zhu, T. Yao, S. Koyama, M.Y. Shen, T. Goto, Appl. Phys. Lett. 70 (1997) 2230.
[5] Z.K. Tang, G.K.L. Wong, P. Yu, M. Kawasaki, A. Ohtomo, H. Koinuma, Y. Segawa, Appl. Phys. Lett. 72 (1998) 3270.
[6] D.M. Bagnall, Y.F. Chen, Z. Zhu, T. Yao, M.Y. Shen, T. Goto, Appl. Phys. Lett. 73 (1998) 1038.
[7] Yefan Chen, D.M. Bagnall, Hang-jun Koh, Ki-tae Park, Kenji Hiraga, Ziqiang Zhu, Takafumi Yao, J. Appl. Phys. 84 (1998) 3912.
[8] Yefan Chen, Hang-Ju Ko, Soon-Ku Hong, Takafumi Yao, Appl. Phys. Lett. 76 (2000) 559.
[9] M. Leroux, N. Grandjean, M. Laugt, J. Massies, B. Gil, P. Lefebvre, P. Bigenwald, Phys. Rev. B 58 (1998) R13371.
[10] P. Waltereit, O. Brandt, A. Trampert, H.T. Grahn, J. Menniger, M. Ramsteiner, M. Reiche, K.H. Ploog, Nature 406 (2000) 865.
[11] B. Gil, P. Lefebvre, T. Bretagnon, T. Guillet, J.A. Sans, T. Taliercio, C. Morhain, Phys. Rev. B 74 (2006) 153302.
[12] J.-M. Chauveau, D.A. Buell, M. Laugt, P. Vennegues, M. Teisseire-Doninelli, S. Berard-Bergery, C. Deparis, B. Lo, B. Vinter, C. Morhain, J. Cryst. Growth 301–302 (2007) 366.
[13] Yasuhiro Kashiwaba, Takami Abe, Akira Nakagawa, Haruyuki Endo, Ikuo Niikura, Yasube Kashiwaba, Phys. Status Solidi A 206 (2009) 944.
[14] T. Abe, Y. Kashiwaba, S. Onodera, F. Masuoka, A. Nakagawa, H. Endo, I. Niikura, Y. Kashiwaba, J. Cryst. Growth 298 (2007) 457.
[15] J.M. Pierce, B.T. Adekore, R.F. Davis, F.A. Stevie, J. Cryst. Growth 283 (2005) 147.
[16] Xi Zhou, Zhao-Xiong Xie, Zhi-Yuan Jiang, Qin Kuang, Shu-Hong Zhang, Tao Xu, Rong-Bin Huang, Lan-Sun Zheng, Chem. Commun. 44 (2005) 5572.
[17] Ulrike Diebold, Lynn Vogel Koplitz, Olga Dulub, Appl. Surf. Sci. 237 (2004) 336.
[18] Wen-Jun Li, Er-Wei Shi, Wei-Zhuo Zhong, Zhi-Wen Yin, J. Cryst. Growth 203 (1999) 186.